

# *In vitro* and *in vivo* degradation of microfiber bioresorbable coronary scaffold

Chi-Hung Huang,<sup>1,2</sup> Sheng-Yang Lee,<sup>2,3</sup> Sonida Horng,<sup>4</sup> Louis-Georges Guy,<sup>4</sup> Ting-Bin Yu<sup>5</sup>

<sup>1</sup>Division of Cardiology, Department of Internal Medicine, Cathay General Hospital, Taipei, Taiwan

<sup>2</sup>School of Dentistry, College of Oral Medicine, Taipei Medical University, Taipei, Taiwan

<sup>3</sup>Dental Department of Taipei Medical University, Wan-Fang Hospital, Taipei, Taiwan

<sup>4</sup>Accellab Inc., Boisbriand, Quebec, J7H 1N8, Canada

<sup>5</sup>DuNing Inc., Tustin, California 92780

Received 4 May 2017; revised 21 August 2017; accepted 28 August 2017

Published online 18 September 2017 in Wiley Online Library (wileyonlinelibrary.com). DOI: 10.1002/jbm.b.33987

**Abstract:** The degradation of Mirage Bioresorbable Microfiber Scaffold was evaluated *in vitro* and *in vivo*. The degradation in polymer molecular weight (MW), strut morphology, and integrity was accessed using gel permeation chromatography (GPC), X-ray micro-computed tomography (micro-CT) evaluation. To simulate the physiological degradation *in vitro*, scaffolds were deployed in silicone mock vessels connected to a peristaltic pumping system, which pumps 37°C phosphate-buffered saline (PBS, pH 7.4) at a constant rate. At various time points (30D, 60D, 90D, 180D, 270D, AND 360D), the MW of microfibers decreased to 57.3, 49.8, 36.9, 13.9, 6.4, and 5.1% against the baseline. The *in vivo* degradation study was performed by implanting scaffolds in internal thoracic arteries (ITAs) of mini-swine. At the scheduled sacrifice time points (30D, 90D, 180D, 270D, 360D, and 540D), the implanted ITAs were excised for GPC analysis; the

MW of the implanted scaffolds dropped to 58.5, 34.7, 24.8, 16.1, 12.9, and 7.1, respectively. Mass loss of scaffolds reached 72.4% at 540D of implantation. Two stages of hydrolysis were observed in *in vitro* and *in vivo* degradation kinetics, and the statistical analysis suggested a positive correlation between *in vivo* and *in vitro* degradation. After 6 months of incubation in animals, significant strut degradation was seen in the micro-CT evaluation in all sections as strut fragments and separations. The micro-CT results further confirmed that every sample at 720D had X-ray transmission similar to surrounding tissue, thereby indicating full degradation within 2 years. © 2017 The Authors. *Journal of Biomedical Materials Research Part B: Applied Biomaterials* published by Wiley Periodicals, Inc. *J Biomed Mater Res Part B: Appl Biomater* 106B: 1842–1850, 2018.

**Key Words:** biomaterials, bioresorbable scaffold, biodegradation, drug-eluting implant, polylactide

**How to cite this article:** Huang, C-H, Lee, S-Y, Horng, S, Guy, L-G, Yu, T-B 2018. *In vitro* and *in vivo* degradation of microfiber bioresorbable coronary scaffold. *J Biomed Mater Res Part B* 2018;106B:1842–1850.

## INTRODUCTION

Percutaneous coronary intervention has evolved over the last 40 years since the plain old balloon angioplasty (POBA) was first introduced to the treatment of coronary artery disease (CAD) in 1977.<sup>1</sup> However, acute coronary occlusion, severe dissection, restenosis, constructive remodeling, and neointimal hyperplasia frequently occurred following POBA.<sup>2,3</sup> To further mitigate the risk of incidence, bare metallic stents (BMS) were developed. BMS was superior to POBA but was still associated with severe neointimal proliferation and long-term restenosis.<sup>4,5</sup> The high risk of in-stent restenosis drove the third revolution in interventional cardiology: drug-eluting stent (DES), which is the most widespread technology in use today and incorporates surface coating that releases anti-proliferative drugs over time.<sup>6</sup> Locally delivered drugs such as sirolimus, rapamycin-derivatives, and paclitaxel delay neointimal formation and consequently restenosis. DES significantly improves the clinical outcome in high-risk patients particularly with complex subsets of lesions.<sup>7</sup>

Early-generation DES contains durable polymer, including polyethylene-covinyl and poly-*n*-butyl methacrylate.<sup>8</sup> The lack of biocompatibility of these permanent polymer coating led to a persistent inflammatory response.<sup>9,10</sup> Newer-generation DES employs thinner strut and more biocompatible polymer to overcome the safety issues associated with early-generation DES. Cobalt chromium alloys with biocompatible polymer (fluoropolymers)<sup>11</sup> or biodegradable polymer (polylactic acid [PLA]/polyglycolic acid)<sup>12</sup> are commonly used in current DES to improve its safety profile. However, primary concerns such as permanent metallic caging, stent fracture, late neointimal response, and stent thrombosis beyond the drug-eluting period are not completely resolved.

With the recent emergence of concerns about the DESs, bioresorbable scaffolds (BRS), which comprise solely biodegradable and biocompatible materials, are considered one of the most promising technologies in interventional cardiology.<sup>13</sup> Ideally, BRSs not only provide immediate acute revascularization but also potentially restore the jailed arteries

**Correspondence to:** T.-B. Yu; e-mail: b.yu@duninginc.com

following the bioresorption process, which may reduce long-term stent thrombosis seen with the DES.<sup>14</sup> Despite the use of biodegradable implants in many medical applications, such as wound closure, dental, orthopedic device, and drug delivery, over the decades, the concept of using BRS in interventional cardiology is still relatively new.

The first BRS used in humans was the Igaki-Tamai scaffold (Kyoto Medical Planning Co., Ltd., Kyoto, Japan), a PLA-based self-expandable device that requires heat treatment.<sup>15</sup> The first in-human study was first conducted in late 1990, and the long-term safety of scaffolds (>10 years) was assessed.<sup>16</sup> Although the results were acceptable, improvements were required to achieve better deliverability and clinical outcome. Following the encouraging results, many BRSs were introduced, and various biodegradable polymers have been used, including PLA,<sup>17,18</sup> poly(lactic-co-glycolic acid) copolymer (PLGA copolymer),<sup>19</sup> salicylate polymer,<sup>20</sup> magnesium,<sup>21</sup> iron,<sup>22</sup> and synthetic polymers.<sup>23</sup> Greater than 15 BRS devices have been developed and evaluated in clinical studies.<sup>24</sup> Most BRSs do not exhibit the same mechanical strength and ductility similar to metallic stents, but their flexibility leads to better conformability and compliance to vessel arteries. Furthermore, the completion of bioresorption restores the vasomotor response to physiological needs, which may promote positive remodeling.<sup>25</sup> Overall, BRSs are a reasonable alternative to DES in noncomplicated cases. Currently, five BRS devices acquired Conformité Européenne approval. Absorb Bioresorbable Vascular Scaffold System (BVS, Abbott Vascular, Santa Clara, CA) has treated >150,000 patients worldwide and has recently received approval from the U.S. Food and Drug Administration (July 2016). However, Abbott Vascular has recently initiated a recall of the Absorb BVS System due to clinical studies showing increased rates of major adverse cardiac events when compared to patients treated with the metallic drug eluting stent at 2 years. The findings conclude that design of current available scaffolds has not yet optimized and there is still room to improve, especially in scaffold degradation and strut thickness. The long scaffold degradation (>2 years) and thick strut (>150  $\mu\text{m}$ ) in small arteries significantly elevate the risk of myocardial infarction and scaffold thrombosis in their later life-cycle stages.

Recently, we presented that a novel bioresorbable drug-eluting scaffold called Mirage Bioresorbable Microfiber Scaffold (Mirage BRMS, Manli Cardiology Singapore) exhibits remarkable mechanical properties and deliverability while demonstrating relatively fast degradation compared with the Absorb BVS system. Mirage BRMS incorporates a distinctive scaffold design and a manufacturing process that involves heat-extruded PLA microfibers. Bioresorbable PLA-based microfibers with strut thicknesses of 125 and 150  $\mu\text{m}$  are braided to deliver a helix coil structure that provides high flexibility and mechanical strength. The low crossing profiles (0.044–0.058 in.) provide great deliverability in operation. They are highly effective in minimizing early vessel recoil and restenosis by offering adequate radial force and eluting anti-proliferative drug sirolimus.<sup>26,27</sup> Overall, Mirage BRMS shows great promise as a next-generation device for treating CAD. In

this study, *in vitro* and *in vivo* degradation of scaffold were evaluated by analyzing the molecular weight (MW) of microfiber. The *in vivo* morphologies of microfibers over time were also assessed by X-ray micro-computed tomography (micro-CT) evaluation. The correlation between *in vitro* and *in vivo* degradation profiles provides a comprehensive understanding of the fate of the device in clinical settings.

## MATERIALS AND METHOD

### Study device and scaffold design

Mirage BRMS is developed for treatment of CAD. It is intended to treat narrowed coronary arteries through three functions: (1) mechanical strength supports the opening of the lumen; (2) sirolimus prevents neointimal growth; and (3) fully bioresorbable materials mitigate the increased long-term risk of stent thrombosis and restenosis seen with traditional stent therapies. The design of Mirage BRMS, which was first proposed by Su et al. in 2001,<sup>28</sup> is unique, and its structure based on continuous multiple microfiber coils provides sufficient strength, flexibility, and compliance. Given the popularity of the PLA copolymer family and their approval for use in clinical applications, Mirage BRMS is fabricated with PLA-based microfiber with a strut thickness of 125  $\mu\text{m}$  in scaffolds with a diameter of  $\leq 3$  mm and a strut thickness of 150  $\mu\text{m}$  in scaffolds with a diameter of  $\geq 3.5$  mm [Figure 3(A)]. Mirage BRMS has low crossing profiles (0.044–0.058 in.) and is 6-F catheter compatible. Microfibers are made of PLA copolymer containing approximately 4% D-lactide and 96% L-lactide. The small number of D-isomers in polymer reduce the crystallinity and accelerate the fiber degradation, while the scaffolds retain their mechanical strength and stiffness. The strength to resist radial compression is comparable to that of commercially available metallic stents made of stainless steel. To reduce neointimal proliferation, the scaffold is coated with a mixture of polylactide and sirolimus at a dose of 9.0  $\mu\text{g}/\text{mm}$ .

Implants made of PLA are not visible under fluoroscopy. Thus, to improve the visibility for positioning or locating the scaffold in arteries, two radiopaque, biocompatible, corrosion-resistant platinum markers are incorporated at both ends of the scaffold. The magnetic resonance imaging (MRI) risk of Mirage BRMS was evaluated to ensure patient safety, and it is demonstrated to be acceptable for a patient undergoing an MRI procedure at 3 T or less.<sup>29</sup>

### *In vitro* degradation and sample MW analysis

To simulate the physiological condition *in vitro*, 3.0 mm (0.005 in. strut thickness) scaffolds were deployed in silicone mock vessels connected to a peristaltic pumping system that constantly pumps 37°C PBS (pH 7.4) at rate of 90 mL/min (1.2 Hz). Silicone mock vessels were purchased from BioEmbedded Research LLC. The performance of the mock vessels is certified and in compliance with ISO 7198. At various time points (30D, 60D, 90D, 180D, 270D, and 360D), six scaffolds retained in the mock vessel were collected and dissolved with 1.0 mL of tetrahydrofuran (THF). The MW of polymers was then determined by using gel permeation chromatography (GPC). The apparatus used for the

GPC analysis is Agilent 1100 G1311A solvent delivery system coupled with G1329A autosampler, 1330A autosampler chiller, G1322 degasser, G1316A column compartment, G1315A reflective index detector, and two Agilent PLgel 5  $\mu\text{m}$  Mixed-D 300  $\times$  7.5 mm GPC columns (manufactured by Agilent, product #0001022104, lot #PL1110-6504). The eluting method used the following conditions: the temperature of the autosampler chiller, the column compartment, and the diode array detector temperature is set at 15, 35, and 35°C, respectively. After sample was transferred into an amber vial placed in the autosampler, 30  $\mu\text{L}$  (injection volume) aliquot of the sample was injected onto the column. The mobile phase is THF, pumped at a 1.00 mL/min flow, leading to a 25 min runtime per sample. The MW of polymer peak in the chromatogram is calculated using Chemstation software and clarity GPC extension against the calibration curve created by polystyrene standard. The parameters  $K$  and  $\alpha$  are  $1.74 \times 10^{-3}$  mL/g and 0.736, respectively. Polystyrene standard (PStQuick Kit-L, Lot# PSQ-KL01N) was purchased from TOSOH Corporation. Those results present MW of PLA relative to polystyrene and they are significantly different to absolute MW obtained in the *in vivo* study. The *in vitro* MW results estimated in bench study are approximately one-fourth of *in vivo* MW results obtained in animal study. Thus, for each time point, MW% was calculated against MW of freshly manufactured BRMS (100%) to compare the MW degradation profile between *in vitro* and *in vivo* studies.

### ***In vivo* implantation**

The scaffold implantation and *in vivo* evaluation were performed in AccellLAB Inc. (Boisbriand, QB, Canada). Mirage BRMS devices were implanted in 25 female or castrated male Yucatan mini-swine coronary arteries and internal thoracic arteries (ITAs). The implanted coronary arteries were used to evaluate safety/efficacy of the Mirage BRMS by angiographic and histological evaluations but the results will be presented in a separate report. This study aims to evaluate the degradation of the Mirage BRMS at various time points and the ITA model shall be considered as an acceptable model for testing *in vivo* BRMS degradation. At time point of 30D, 90D, 180D, 270D, 360D, 540D, and 720D, all implanted animals that survived until the scheduled termination was sacrificed. At only the 30D time point, at the scheduled sacrifice day, a total of 12 new Mirage BRMS were implanted proximally to the previously implanted scaffold in the ITAs. These scaffolds were collected on the same day as the 0D cohorts. Following euthanasia, ITAs were excised and flushed with lactated Ringer's solution. The arteries selected for MW measurement were flash frozen in liquid nitrogen and kept on dry ice prior to being stored in a  $-80^\circ\text{C}$  freezer. Scaffolded arteries selected for micro-CT evaluation were fixed in 10% neutral-buffered formalin (NBF).

### ***In vivo* MW and mass analysis**

To evaluate *in vivo* scaffold degradation in the ITAs, MW measurements using GPC were performed in PolyAnalytik

Inc (London, ON, Canada). The following procedure was followed for the sample preparation: the complete artery implanted scaffold was first rinsed with 20% ethanol solution (v/v) to wash residual blood from the sample. The artery implanted scaffold was cut into fine pieces using a sharp sterilized blade to expose the implanted scaffold. The resulting sample, which contained artery and scaffold, was then submerged in 2 mL of dissolution solvent chloroform and left to dissolve under gentle rocking for 24 h at room temperature. The sample was filtered into an autosampler vial through 0.22  $\mu\text{m}$  PTFE syringe filter and prepared for MW analysis. In the measurement, the Viscotek GPC system (Malvern) was equipped with an oven that houses four detectors: refractive index (RI), ultraviolet (UV), right-angle and low-angle light scattering (RALS/LALS), and four-capillary differential viscometer. The analytical method employs the mobile phase of 0.05M potassium trifluoroacetate in 1,1,1,3,3,3-hexafluoro-2-propanol, and size exclusion columns packed with styrene-divinylbenzene. Poly(methyl methacrylate) was used as calibration standards. The UV absorption of polymer was used to determine the concentration of PLA and calculate the scaffold mass.

### **Micro-CT evaluation**

Selected scaffolded arteries for micro-CT were transferred from NBF to 100% alcohol and scanned using a Skyscan 1172 micro-CT model at a regular resolution. The long axis of the device was aligned perpendicularly to the axis of the X-ray beam. Constant settings for X-ray energy and image capture were maintained for the entire study duration. The obtained projection images were processed with the NRecon image reconstruction software using a convolution and back projection algorithm to produce a stack of 8-bit BMP images, each one of them representing a slice of the sample. Finally, a full three-dimensional (3D) model and animation was generated for visualization of the scaffold. The scaffolds scanned by micro-CT were analyzed using the following scoring system:

Strut discontinuity

0 = Absent

1 = Evaluated at  $\leq 10$  strut breaks

2 = Evaluated at  $> 10$  and  $\leq 25$  strut breaks

3 = Evaluated at  $> 25$  and  $\leq 150$  strut breaks

4 = Evaluated at  $\geq 150$  strut breaks

The degree of micro-CT X-ray transmission grading scale as a surrogate for resorption

0 = No change in X-ray transmission compared with baseline

1 = Mild decrease in X-ray transmission compared with baseline but stronger than surrounding tissue; 2 = Moderate decrease in X-ray transmission compared with baseline but stronger than surrounding tissue

3 = X-ray transmission similar to surrounding tissue

(Note: Baseline corresponds to the acute time point, and the degree of X-ray transmission for the acute time point was compared with the surrounding tissues)

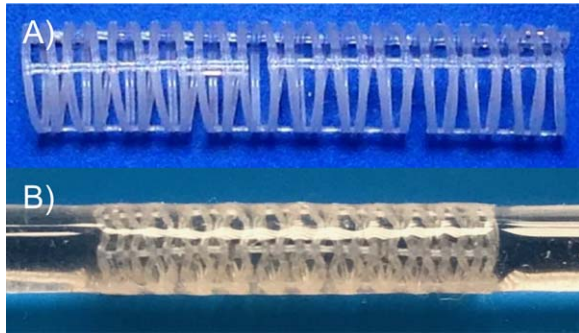


**FIGURE 1.** Mirage BRMS deployed in silicon mock vessel for *in vitro* degradation. (A) Intact Mirage BRMS and (B) scaffold deployed in the vessel.

## RESULTS

### *In vitro* MW analysis

To mimic the physiological condition *in vitro*, Mirage BRMS devices were deployed in the silicone mock vessels connected to the peristaltic pumping system that constantly pumps PBS buffer (Figure 1). The silicon mock vessels and pulses generated by the peristaltic pump simulated the cardiovascular arteries and their contractions yielded by heartbeats, while the PBS heated at 37°C mimicked the fluidic environments. At each time point, scaffolds were recovered, and the MW of microfibers was determined using calibration curve created by polystyrene standards. The representative GPC chromatograms of PLA polymers at various time points are shown in Figure 2. As the incubation proceeded, polymer MW decreased and polydispersity (PDI) increased

**TABLE I.** *In Vitro* MW Measurement Results of Scaffolds at Various Time Points

Day	Mn <sup>a</sup>		PDI	MW % <sup>b</sup>
	Ave.	RSD%		
0	204,216	8.4	1.894	100.0
30	116,939	2.2	2.154	57.3
60	106,397	9.9	2.210	49.8
90	101,793	11.1	2.340	36.9
180	75,441	2.4	3.529	13.9
270	28,362	5.4	5.988	6.4
360	13,022	4.8	3.758	5.1

<sup>a</sup> MW was determined by GPC coupled with RID detector and the MW results are relative to polystyrene standards.

<sup>b</sup> MW percentage (MW%) is calculated against day-0 according to the number average MW (Mn) results.

(Table I). After 360 d of incubation, quantitative characterization indicated that the MW of microfibers decreased to 5.1% (MW of approximately 10,500) compared with those of freshly prepared samples, which have a MW of approximately 200,000. A notable detail is that significant breakdown of scaffold fibers within the mock vessels was observed at 270D and 360D time points (especially for the 360D group). Partial sample loss into the circulation system during the incubation cannot be avoided. Thus, the quantitative results for MW and PDI may not be representative for the samples collected at those time points (270D and 360D).

The hydrolysis rate of amorphous polylactide has a slow-to-fast transition at a certain MW (Mn).<sup>30</sup> The polymer

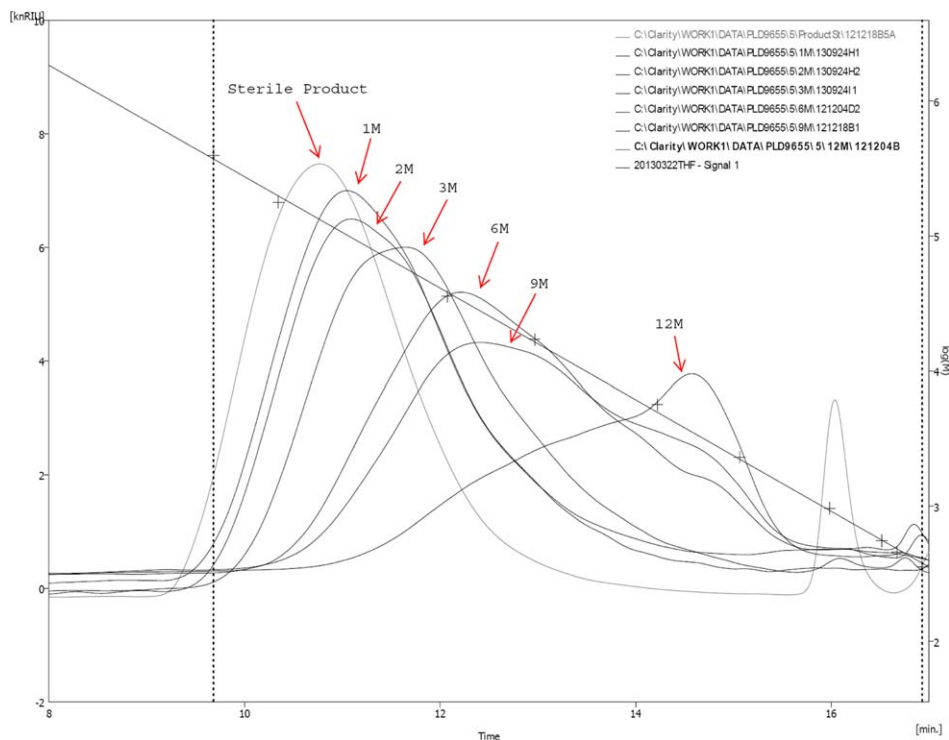


**FIGURE 2.** Representative chromatograms of Mirage scaffolds subjected to various incubation durations (0D, 30D, 60D, 90D, 180D, 270D, and 360D).

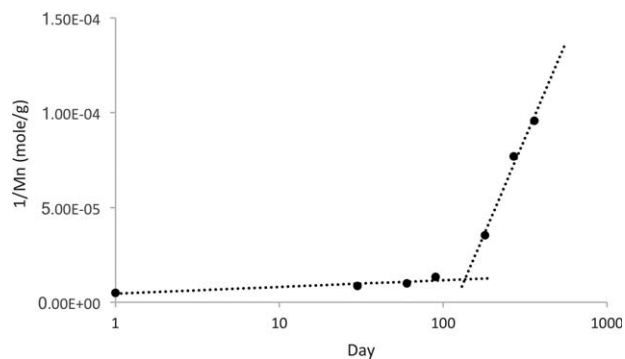


**FIGURE 3.** *In vitro* degradation kinetics of PLA for Mirage BRMS (inverse of the number average MW vs. the logarithm of degradation time).

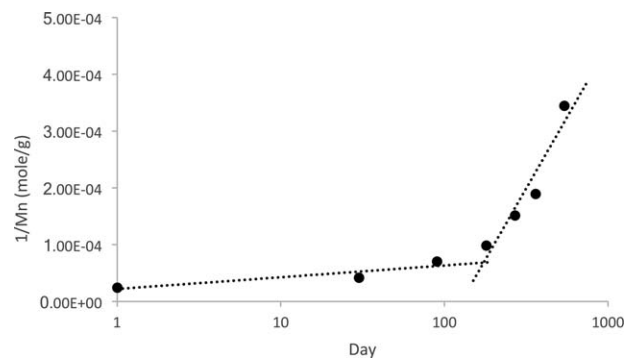


**FIGURE 4.** *In vivo* degradation kinetics of PLA for Mirage BRMS (inverse of the number average MW vs. the logarithm of degradation time).

chain end does not promote the hydrolysis of the sample until their MW reaches a critical point. Thus, we probed the degradation kinetics of PLA in BRMS by plotting the inverse number average MW [ $1/M_n(t)$ ] against the logarithm of the incubation duration  $\log(t)$  (Figure 3).<sup>31</sup> Results indicate that the hydrolysis goes through two kinetic processes with different rates. Initially, the PLA device degraded at a constant rate, and  $1/M_n$  increased linearly as the degradation time prolonged. When the hydrolysis proceeded and  $M_n$  reached a critical point, the hydrolysis accelerated and led to a higher degradation rate in the plot. The hydrolysis rate is speculated to change at approximately 120D because of the possible concentration increase in chain end groups (-COOH) that catalyzed the hydrolysis.<sup>32</sup> Those newly produced chain ends can effectively hydrolyze the ester bond in part of the samples through diffusion.

### ***In vivo* MW and mass analysis**

BRMS *in vivo* evaluation and device implantation were performed in 25 female or castrated male Yucatan mini-swine ITAs. The MW measurements of the Mirage BRMS were conducted at 30D, 90D, 180D, 270D, 360D, and 540D time points. At each time point, all implanted animals were sacrificed, and the ITAs were harvested. The resulting arteries that contained scaffolds were submerged in dissolution solvent and shaken for 24 h. Several dissolution solvents were

tested; chloroform shows the maximum PLA recovery without other interfering impurities.

Triple detection GPC method employs detectors of RI, UV, RALS/LALS, and four-capillary differential viscometer to obtain the absolute MWs of PLA. The RI detector is employed to calculate the PLA concentration, refractive index increment, and injection recovery. The UV detector is used to detect organic interference due to proteins, DNA, or RNA in the artery implanted PLA scaffold samples. The viscometer delivers the dilute solution properties, including intrinsic viscosity ( $\eta$ ), hydrodynamic radius ( $R_h$ ), and conformational, and structural parameters. The MW parameters, including  $M_n$ ,  $M_w$ , and  $M_z$ , were determined from the RALS detector using an average  $dn/dc$  value of  $0.153 \pm 0.011$  mL/g. This  $dn/dc$  value is the average value calculated assuming 100% recovery of each injection of the different virgin PLA scaffolds with and without drug.

Table II represents the results for *in vivo* MW measurement of scaffolds at various time points. The initial MW of the scaffold was approximately 86 000 Da ( $M_w$ ) and approximately 41 000 Da ( $M_n$ ). The MW of scaffolds decreased to 58.5, 34.7, 24.8, 16.1, 12.9, and 7.1% at 30D, 90D, 180D, 270D, 360D, and 540D, respectively. The degradation kinetics of PLA was evaluated by plotting the inverse number average MW ( $1/M_n$ ) against the logarithm of incubation duration (Figure 4). Similar to the *in vitro*

**TABLE II. *In Vivo* MW Measurement Results of Scaffolds at Various Time Points**

Day	Absolute MW <sup>a</sup>					Relative MW <sup>b</sup>			
	Mn		Mw		PDI	Mn			MW % <sup>c</sup>
	Ave.	RSD%	Ave.	RSD%		Ave.	RSD%	PDI	
0	40,896	100.0	85,842	4.3	2.108	72,122	3.9	1.919	100.0
30	23,937	58.5	46,844	6.5	1.966	34,469	8.5	2.315	58.5
90	14,195	34.7	30,965	4.8	2.184	19,984	7.6	2.596	34.7
180	10,133	24.8	22,598	2.6	2.232	14,324	3.9	2.590	24.8
270	6602	16.1	15,715	6.8	2.394	8583	5.3	2.909	16.1
360	5274	12.9	12,581	6.8	2.405	5940	11.9	3.315	12.9
540	2899	7.1	6158	10.9	2.122	4149	8.0	2.132	7.1

<sup>a</sup> Results were determined by GPC and RALS/LALS detector. The results represent the absolute MWs of PLA.

<sup>b</sup> Results were determined by GPC coupled with RID detector and the MW results are relative to poly(methyl methacrylate).

<sup>c</sup> MW percentage (MW%) is calculated against day-0 according to the number average MW ( $M_n$ ) results from RALS/LALS detector.

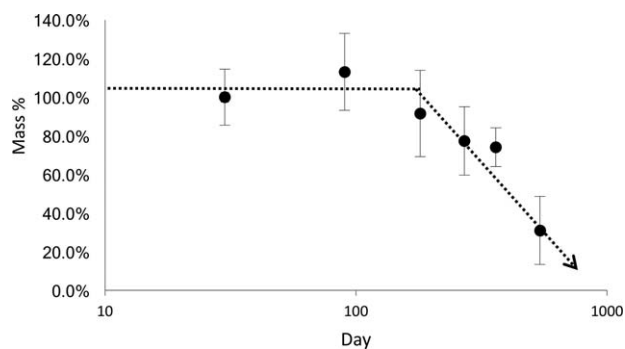


**FIGURE 5.** *In vivo* weight mass percentage (%) of PLA for Mirage BRMS.

degradation kinetics shown in Figure 3, two stages of hydrolysis were observed. Change in MW (Mn) decreased at approximately 160D to 180D. Following the change in hydrolysis rate, mass loss started; a mass loss of 22.6% was observed at 270D. After 540D of incubation in animals, approximately 30% PLA mass was retained in the harvested arteries (Figure 5). Given the dramatic mass loss in this period, the Mirage BRMS device is suggested to be completely degraded within 2 years after implantation. These results confirm that the degradation patent of PLA in Mirage BRMS is similar to that of PLA used in Elixir DESolve Device; their resorption process takes 18–24 months.<sup>33,34</sup>

### Micro-CT evaluation study

Micro-CT, a recently developed technology, has been extensively used to explore the 3D micromorphology in tissue engineering application.<sup>35–37</sup> Micro-CT provides numerous advantages to quantifying complex geometries in 3D biological samples, including (1) contactless technique and nondestructive to internal structure; (2) high resolution (10  $\mu\text{m}$ ) and contrast sensitivity compared with ultrasound (30  $\mu\text{m}$ ) and magnetic resonance imaging (100  $\mu\text{m}$ ); and (3) any spatial location of the interior structure can be isolated. We employed micro-CT to evaluate the strut integrity through time in the *in vivo* study. The ITAs of Yucatan mini-swine pigs were implanted with BRMS scaffolds. After incubation in the animals for various durations, the scaffolded ITAs were harvested and divided into a series of two-dimensional (2D) slices. The iodine-stained slices were scanned with a SkyScan 1172 micro-CT system. The resultant 2D images correlated to the material density revealed the material phases within the specimen. Images were reconstructed in 3D using software. The strut discontinuity (strut break counts) and X-ray transmission were evaluated (Table III).

## DISCUSSION

### PLA degradation and *in vitro/in vivo* MW correlation

Three stages of PLA polymer degradation were proposed by Hakkarainen et al.<sup>38</sup> During the first phase, the water diffusion process dominates the polymer degradation. Polymers degrade, and their MW decreases without significant mass

**TABLE III. Summary of Micro-CT Images of Mirage BRMS-Implanted Swine Arteries**

		Strut Discontinuity Mean $\pm$ SD	Degree of Micro-CT X-Ray Transmission Mean $\pm$ SD
Acute	$n = 4$	$0.50 \pm 0.58$	$0.25 \pm 0.50$
30D	$n = 4$	$0.75 \pm 0.50$	$0.50 \pm 0.58$
90D	$n = 4$	$2.25 \pm 0.50$	$0.00 \pm 0.00$
180D	$n = 4$	$3.00 \pm 0.00$	$0.25 \pm 0.50$
270D	$n = 4$	$3.00 \pm 0.00$	$0.25 \pm 0.50$
360D	$n = 4$	$3.00 \pm 0.00$	$0.00 \pm 0.00$
540D	$n = 4$	$4.00 \pm 0.00$	$2.25 \pm 0.50$
720D	$n = 4$	– <sup>a</sup>	$3.00 \pm 0.00$

<sup>a</sup> Not evaluated

loss. When polymer degradation enters the second phase, mass loss starts, and polymers are hydrolyzed into soluble oligomers that have an MW of 2–3 kDa. However, the MW change decelerates during this stage. The third phase starts as the total mass loss is reached and all oligomers are completely hydrolyzed and resorbed. Polylactide copolymer is believed to degrade in the body mostly through the hydrolytic degradation. The resulting lactic acids, which are naturally occurring products in the body, are subsequently metabolized and eliminated into  $\text{CO}_2$  and  $\text{H}_2\text{O}$  through the Krebs cycle.<sup>39</sup>

In this study, the three stages of degradation are also seen in Mirage BRMS made of PLA. After the implantation, the hydrolysis and degradation of polymer start, but no physical change was observed in the first 120D to 180D of incubation. Between 180D and 540D, PLA scaffolds proceed to the second stage *in vitro* and *in vivo*. The devices accomplished their functions, and the change in their MW slowed down. During this stage, the MW of microfibers decreased to approximately 3000 Da, and significant weight loss was observed. The degradation enters the third stage after 540D, and total mass loss is reached.

The *in vitro* and *in vivo* MW degradation profiles of Mirage BRMS are presented in Figure 6. The *in vitro* degradation was faster than *in vivo* degradation after 180D likely because of the low permeability of polymer to the water of the blood flow after the scaffolds were completely covered by endothelialization. These results confirmed that the

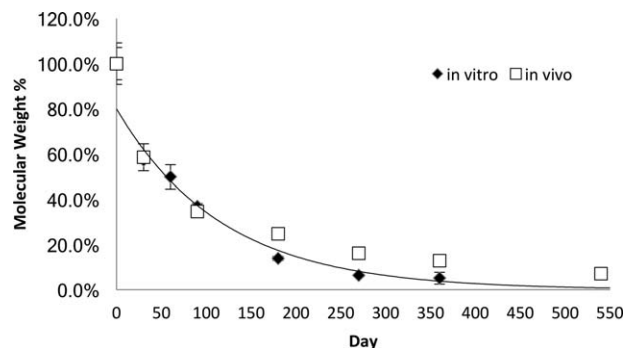


**FIGURE 6.** *In vivo* and *in vitro* degradation profile of PLA for Mirage BRMS.

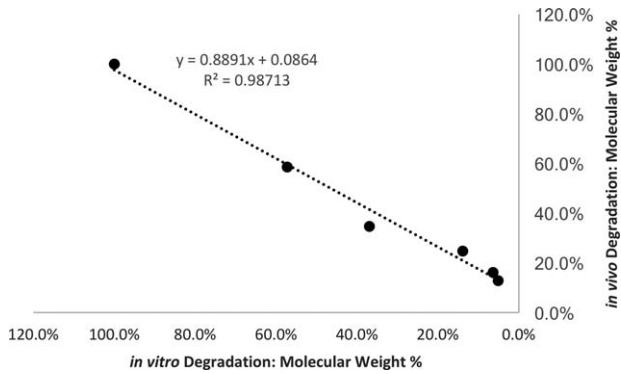


**FIGURE 7.** *In vivo* and *in vitro* correlation of PLA degradation in Mirage BRMS.

water contact or liquid flow might affect the bulk degradation of the polymers significantly. Overall, the statistical analysis may suggest a positive and linear correlation between *in vivo* and *in vitro* degradation as the correlation coefficient is high (Figure 7).

### Strut integrity and x-ray transmission

Micro-CT analysis of 32 BRMS from various time points (acute to 720D) revealed patent arteries. While the MW analysis indicates that BRMS has a faster degradation profile compared with BVS, the micro-CT 3D images confirm few strut breaks at acute, 30D, and 90D despite the fast degradation and good conformation of the scaffolded arteries for 180D (Figure 8). Strut discontinuity evaluation revealed that MMSE strut break counts remained low at acute, 30D, and 90D (Figure 9). The number of strut breaks increased significantly once the devices entered the second stage of degradation. For the scaffolds of 180D, 270D, and 360D, every scaffold had >25 and ≤150 strut breaks, while for the 540D scaffold, three scaffolds were evaluated at ≥150 strut breaks. Strut discontinuity could not be evaluated in 720D as the scaffolds were not visible enough to perform the evaluation (X-ray transmission similar to surrounding tissue).

No significant change of X-ray transmission compared with baseline (acute time point) was observed in the first 360D. Some scaffolds had a mild decrease in X-ray transmission compared with the baseline, but the transmission was stronger than that of surrounding tissue in the 30D and 180D scaffolds. The 540D scaffolds exhibited X-ray transmission that decreased moderately compared with the baseline but was stronger than that of surrounding tissue; one scaffold had X-ray transmission similar to surrounding tissue. For the 720D cohort, every sample had X-ray transmission similar to surrounding tissue. Overall, the degree of X-ray transmission seemed to decrease with time from the acute to the 720D time point. These strut discontinuity and transmission numbers confirmed that Mirage BRMS offers a solution for faster vessel restoration while providing sufficient support and integrity within the first 180days (6 months) of implantation.

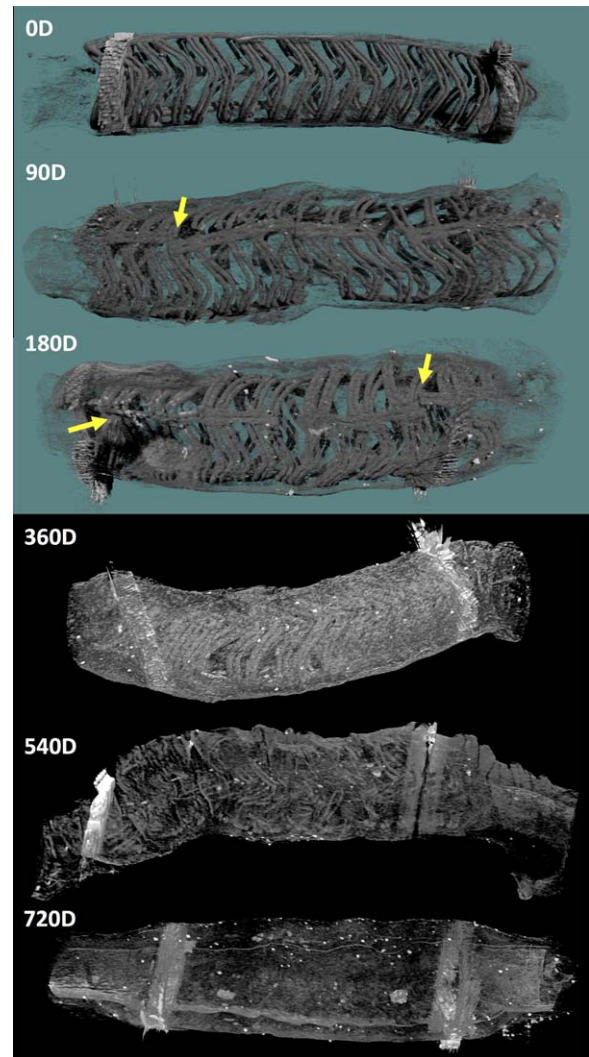


**FIGURE 8.** Representative micro-CT images of Mirage BRMS revealing an open scaffold at 0D, 180D, 360D, 540D and 720D. Radiopaque markers at both extremities of the scaffold create blooming artifacts under micro-CT imaging for PLA. Yellow arrows indicate strut breakages.

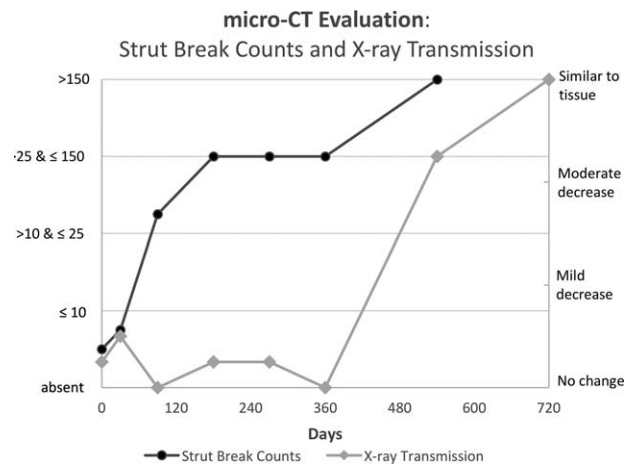


**FIGURE 9.** Strut break counts and X-ray transmission from micro-CT images of Mirage BRMS-implanted swine arteries.

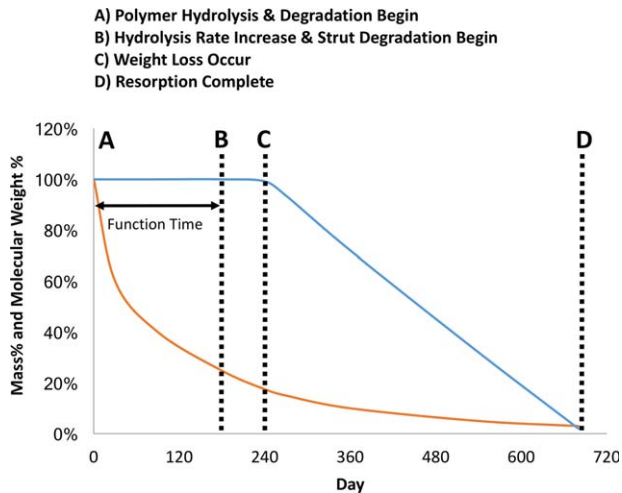


FIGURE 10. Proposed degradation profile of Mirage BRMS.

## CONCLUSIONS

The degradation of Mirage BRMS scaffolds was evaluated *in vitro* and *in vivo*. The polymer MW and strut morphology were accessed using GPC, and micro-CT evaluation. The MW measurement results elucidated that a positive and linear correlation in polymer degradation exists between *in vitro* and *in vivo*, even though a faster degradation was seen in samples incubated in animals. Upon combining the micro-CT and GPC findings, we proposed a two-stage model of Mirage BRMS degradation [(A,B) and (B–D) in Figure 10]. After the scaffolds were implanted (point A), the hydrolysis began, which was governed by water diffusion. At the time point of approximately 180D (point B), the hydrolysis rate increased dramatically, and degradation entered the second stage. During this stage, significant strut degradations were observed in the micro-CT evaluation, confirming the occurrence of tissue integration and scaffold resorption. Scaffold mass decreased significantly between the period of 270D and 540D, and micro-CT evaluation suggest a complete degradation within 720D of incubation.

## ACKNOWLEDGMENTS

We acknowledge Manli Cardiology, Singapore for research grand support. We acknowledge to Mr. Eric Landry (PolyAnalytik Inc., ON, Canada) for the MW analysis studies support. We acknowledge AccelLAB Inc. (Boisbriand, QB, Canada) for pre-clinical research support.

## DISCLOSURE

All authors have reported that they have no relationships relevant to the contents of this paper to disclose.

## REFERENCES

- Grüntzig A. Transluminal dilatation of coronary artery stenosis—experimental report. In: Zeitler E, Grüntzig A, Schoop W (eds) Percutaneous Vascular Recanalization. Berlin/Heidelberg: Springer; 1978. pp 57–65.
- Roubin GS, Douglas JS, King SB, Lin SF, Hutchison N, Thomas RG, Gruentzig AR. Influence of balloon size on initial success, acute complications, and restenosis after percutaneous transluminal coronary angioplasty. A prospective randomized study. *Circulation* 1988;78(3):557–565.
- Sigwart U, Urban P, Golf S, Kaufmann U, Imbert C, Fischer A, Kappenberger L. Emergency stenting for acute occlusion after coronary balloon angioplasty. *Circulation* 1988;78(5):1121–1127.
- Serruys PW, de Jaegere P, Kiemeneij F, Macaya C, Rutsch W, Heyndrickx G, Emanuelsson H, Marco J, Legrand V, Materne P, Belardi J. A comparison of balloon-expandable-stent implantation with balloon angioplasty in patients with coronary artery disease. *N Engl J Med* 1994;331(8):489–495.
- Fischman DL, Leon MB, Baim DS, Schatz RA, Savage MP, Penn I, Detre K, Veltri L, Ricci D, Nobuyoshi M, Cleman M. A randomized comparison of coronary-stent placement and balloon angioplasty in the treatment of coronary artery disease. *N Engl J Med* 1994;331(8):496–501.
- Htay T, Liu MW. Drug-eluting stent: a review and update. *Vasc Health Risk Manage* 2005;1(4):263.
- Capodanno D, Dipasqua F, Tamburino C. Novel drug-eluting stents in the treatment of de novo coronary lesions. *Vasc Health Risk Manage* 2011;7:103.
- Moses JW, Leon MB, Popma JJ, Fitzgerald PJ, Holmes DR, O’Shaughnessy C, Caputo RP, Kereiakes DJ, Williams DO, Teirstein PS, Jaeger JL. Sirolimus-eluting stents versus standard stents in patients with stenosis in a native coronary artery. *N Engl J Med* 2003;349(14):1315–1323.
- Virmani R, Farb A, Guagliumi G, Kolodgie FD. Drug-eluting stents: caution and concerns for long-term outcome. *Coronary Artery Dis* 2004;15(6):313–318.
- Hezi-Yamit A, Sullivan C, Wong J, David L, Chen M, Cheng P, Shumaker D, Wilcox JN, Udipi K. Impact of polymer hydrophilicity on biocompatibility: implication for DES polymer design. *J Biomed Mater Res Part A* 2009;90(1):133–141.
- Sheiban I, Villata G, Bollati M, Sillano D, Lotrionte M, Biondi-Zoccai G. Next-generation drug-eluting stents in coronary artery disease: focus on everolimus-eluting stent (Xience V®). *Vasc Health Risk Manage* 2008;4(1):31.
- Pendyala LK, Matsumoto D, Shinke T, Iwasaki T, Sugimoto R, Hou D, Chen JP, Singh J, King SB, Chronos N, Li J. Nobori stent shows less vascular inflammation and early recovery of endothelial function compared with Cypher stent. *JACC: Cardiovasc Interv* 2012;5(4):436–444.
- Onuma Y, Serruys PW. Bioresorbable scaffold the advent of a new era in percutaneous coronary and peripheral revascularization? *Circulation* 2011;123(7):779–797.
- Indolfi C, De Rosa S, Colombo A. Bioresorbable vascular scaffolds [mdash] basic concepts and clinical outcome. *Nat Rev Cardiol* 2016;13:719–729.
- Tamai H, Igaki K, Kyo E, Kosuga K, Kawashima A, Matsui S, Komori H, Tsuji T, Motohara S, Uehata H. Initial and 6-month results of biodegradable poly-L-lactic acid coronary stents in humans. *Circulation* 2000;102(4):399–404.
- Nishio S, Kosuga K, Igaki K, Okada M, Kyo E, Tsuji T, Takeuchi E, Inuzuka Y, Takeda S, Hata T, Takeuchi Y. Long-term (>10 years) clinical outcomes of first-in-human biodegradable poly-L-lactic acid coronary stents Igaki-Tamai stents. *Circulation* 2012;125(19):2343–2353.
- Serruys PW, Onuma Y, Ormiston JA, de Bruyne B, Regar E, Dudek D, Thuesen L, Smits PC, Chevalier B, McClean D, Koolen J. Evaluation of the second generation of a bioresorbable everolimus drug-eluting vascular scaffold for treatment of de novo coronary artery stenosis six-month clinical and imaging outcomes. *Circulation* 2010;122(22):2301–2312.
- Wiebe J, Bauer T, Dorr O, Mollmann H, Ham CW, Nef HM. Implantation of a novolimus-eluting bioresorbable scaffold with a strut thickness of 100  $\mu\text{m}$  showing evidence of self-correction. *EuroIntervention* 2015;11:204.
- Venkatraman SS, Tan LP, Joso JF, Boey YC, Wang X. Biodegradable stents with elastic memory. *Biomaterials*. 2006;27(8):1573–1578.
- Jabara R, Pendyala L, Geva S, Chen J, Chronos N, Robinson K. Novel fully bioabsorbable salicylate-based sirolimus-eluting stent. *EuroIntervention* 2009;5:F58–F64.
- Chen Y, Xu Z, Smith C, Sankar J. Recent advances on the development of magnesium alloys for biodegradable implants. *Acta Biomater* 2014;10(11):4561–4573.

22. Wu C, Qiu H, Hu XY, Ruan YM, Tian Y, Chu Y, Xu XL, Xu L, Tang Y, Gao RL. Short-term safety and efficacy of the biodegradable iron stent in mini-swine coronary arteries. *Chin Med J* 2012;126(24):4752–4757.
23. de Ribamar Costa J, Abizaid A, Chamie D, Lansky A, Kochman J, Koltowski L. Initial results of the fantom 1 trial: A first-in-man evaluation of a novel, radiopaque sirolimus-eluting bioresorbable vascular scaffold. *J Am Coll Cardiol* 2016;67(13S):232.
24. Tenekecioglu E, Farooq V, Bourantas CV, Silva RC, Onuma Y, Yilmaz M, Serruys PW. Bioresorbable scaffolds: a new paradigm in percutaneous coronary intervention. *BMC Cardiovasc Disorders* 2016;16(1):1.
25. Brugaletta S, Heo JH, Garcia-Garcia HM, Farooq V, van Geuns RJ, de Bruyne B, Dudek D, Smits PC, Koolen J, McClean D, Dorange C. Endothelial-dependent vasomotion in a coronary segment treated by ABSORB everolimus-eluting bioresorbable vascular scaffold system is related to plaque composition at the time of bioresorption of the polymer: indirect finding of vascular reparative therapy?. *Eur Heart J* 2012;33(11):1325–1333.
26. Santoso T, Liew HB, Tenekecioglu E, Costa R, Chamie D, Su S, Abizaid A, Bourantas C, Torii R, Onuma Y, Serruys P. TCT-431 randomized comparison of absorb bioresorbable vascular scaffold and mirage microfiber sirolimus eluting scaffold using multi-modality imaging. *J Am Coll Cardiol* 2016;68(18S):B174.
27. Tenekecioglu E, Serruys PW, Onuma Y, Costa R, Chamie C, Sotomi Y, Yu T-B, Abizaid A, Liew HB, Santoso T. Randomized comparison of ABSORB bioresorbable vascular scaffold and Mirage microfiber sirolimus-eluting scaffold using multi-modality imaging. *J Am Coll Cardiol Interv.* 2017;10(11):1115–1130.
28. Su SH, Chao RY, Landau CL, Nelson KD, Timmons RB, Meidell RS, Eberhart RC. Expandable bioresorbable endovascular stent. I. Fabrication and properties. *Ann Biomed Eng* 2003;31(6):667–677.
29. Shellock FG, Giangarra CJ. In vitro assessment of 3-T MRI issues for a bioabsorbable, coronary artery scaffold with metallic markers. *Magn Reson Imaging* 2014;32(2):163–167.
30. Lyu S, Schley J, Loy B, Lind D, Hobot C, Sparer R, Untereker D. Kinetics and time-temperature equivalence of polymer degradation. *Biomacromolecules* 2007;8(7):2301
31. Albertsson AC, Eklund M. Influence of molecular structure on the degradation mechanism of degradable polymers: In vitro degradation of poly (trimethylene carbonate), poly (trimethylene carbonate-co-caprolactone), and poly (adipic anhydride). *J Appl Polym Sci* 1995;57(1):87–103.
32. Lyu S, Sparer R, Untereker D. Analytical solutions to mathematical models of the surface and bulk erosion of solid polymers. *J Polym Sci Part B* 2005;43(4):383–397.
33. Costopoulos C, Naganuma T, Latib A, Colombo A. Looking into the future with bioresorbable vascular scaffolds. *Expert Rev Cardiovasc Ther* 2013;11(10):1407–1416.
34. Abizaid A, Costa RA, Schofer J, Ormiston J, Maeng M, Witzenbichler B, Botelho RV, Costa JR, Chamie D, Abizaid AS, Castro JP. Serial multimodality imaging and 2-year clinical outcomes of the novel DESolve novolimus-eluting bioresorbable coronary scaffold system for the treatment of single de novo coronary lesions. *JACC: Cardiovasc Interv* 2016;9(6):565–574.
35. Stock SR. Recent advances in X-ray microtomography applied to materials. *Int Mater Rev* 2008;53(3):129–181.
36. Barbeta A, Bedini R, Pecci R, Dentini M. Role of X-ray microtomography in tissue engineering. *Ann Ist Super Sanita* 2012;48(1):10–18.
37. Watling CP, Lago N, Benmerah S, FitzGerald JJ, Tarte E, McMahon S, Lacour SP, Cameron RE. Novel use of X-ray micro computed tomography to image rat sciatic nerve and integration into scaffold. *J Neurosci Methods.* 2010;188(1):39–44.
38. Hakkarainen M, Albertsson AC, Karlsson S. Weight losses and molecular weight changes correlated with the evolution of hydroxyacids in simulated in vivo degradation of homo-and copolymers of PLA and PGA. *Polym Degrad Stab* 1996;52(3):283–291.
39. Engineer C, Parikh J, Raval A. Review on hydrolytic degradation behavior of biodegradable polymers from controlled drug delivery system. *Trends Biomater Artif Organs* 2011;25(2):79–85.